

ORIGINAL ARTICLE

Fluid Structure Interaction of Renal Arteries of Abdominal Aorta Subjected to Single and Double Stenosed Complication

Adi Azriff Basri^{1,5}, S.M Abdul Khader², Cherian Johny², Raghuvir Pai B², Mohammed Zuber³, Zainuldin Ahmad⁴, Kamarul Arifin Ahmad^{1,5}

¹ Department of Aerospace Engineering, Faculty of Engineering, Universiti Putra Malaysia, 43400 Serdang, Selangor, Malaysia.

² Department of Mechanical and Manufacturing Engineering, Manipal Institute of Technology, Manipal Academy of Higher Education, Manipal, 576104, Karnataka, India.

³ Department of Aeronautical and Automobile Engineering, Manipal Institute of Technology, Manipal Academy of Higher Education, Manipal, 576104, Karnataka, India.

⁴ Department of Mechanical Engineering, School of Science and Engineering, Manipal International University, Malaysia, 71800, Nilai, Negeri Sembilan, Malaysia.

⁵ Aerospace Malaysia Research Center (AMRC), Universiti Putra Malaysia, 43400 Serdang, Selangor, Malaysia

ABSTRACT

Introduction: In this study, Renal artery (RA) stenosis of Single Stenosed (SS) and Double Stenosed (DS) with the condition of Normal Blood Pressure (NBP) and High Blood Pressure (HBP) were investigated using the aid of Fluid Structure Interaction (FSI) approach. **Methods:** Numerical analysis of 3D model patient's specific abdominal aorta with RA stenosis was conducted using FSI solver in software ANSYS 18. **Results:** The results of velocity profile, pressure drop, time average wall shear stress (TAWSS), Oscillatory shear index (OSI) and total deformation of SS and DS with the condition of NBP and HBP were compared in terms of blood flow and structural wall tissue behaviour. The results concluded SS-NBP produced the highest value of velocity profile, TAWSS and OSI parameter compared to the others. Meanwhile, SS-HBP indicates the highest value pressure drop. On the other hand, SS-HBP and DS-HBP have a higher distribution of deformation contour and also maximum VMS compared to SS-NBP and DS-HBP. **Conclusion:** With the aid of FSI approach, this studied has proven that the existence of SS at RA location has a higher impact on the velocity magnitude, higher pressure drop, higher TAWSS and OSI value compared to the DS case. This is due to a high concentration of pressure acting at the narrow blood vessel of SS compared to DS cases which most of the blood flow will pass to the lower part of abdominal aorta.

Keywords: Fluid Structure Interaction, Renal artery, Stenosis, Renal artery stenosed, Hemodynamics blood flow

Corresponding Author:

Adi Azriff Bin Basri, PhD

Email: adiazriff@upm.edu.my

Tel: + 603-9769 4392

INTRODUCTION

One of the principal causes of kidney failure is renal artery (RA) stenosis where the stenosis restrain the blood supply and narrowing arteries size which obstruct blood flows through the blood vessel towards the kidney. Hence, these circumstances lead to the reduction of oxygenated blood volume to the kidney and may cause the failure of the kidney where it is a crucial issue as it linked with secondary hypertension (1). According to Bokhari et. al (2), RA stenosis is highlighted as the major cause of hypertension in 1% to 10% of the 50 million of United States citizen (3). The RA stenosis has also reduced the mass flow rate of the blood flow but increased the blood flow pressure and velocity due to

the acute area of the blood vessel (4,5). Mortazavinia et al. (6) have proven the angulation of stenosed at RA subjected to the changes of velocity and mass flow of blood flow lead to hypertension complication. Kagadis et al. (7) investigated the clinical effects of RA stenosis on flow dynamics and vessel wall based on patient specific data, whereby the presence of RA stenosis increased the flow resistance and lead to lower blood flow rates.

Nowadays, with the emerging technology specifically on coupling technique between numerical simulation and clinical imaging, researchers around the world had conducted thousands of simulations study to understand detailed of blood flow behavior specifically in understanding the mechanism of stenosis development in patient (7–11). Computational Fluid Dynamics (CFD) and Fluid Structure Interaction (FSI) techniques are parts of the numerical simulation approach for researches to investigate the blood flow behavior of cardiovascular disease. The simulation technique provides a non-

invasive study of blood velocity, pressure and shear stress which the detail assessment for the hypothesis of disease formation can be obtained. Moreover, this novel simulation technique also can be used to as an intravascular devices prior to performing in-vivo implementation (7,12).

For example, Hussain et. al. (13) investigated the effect of different inlet diameter of aorta coronary sinus conduit with respect to the pressure drop from 80 mmHg to 15 mmHg using ANSYS simulation software. The authors compared the pressure reduction pattern as well as velocity distribution in each model. Basri et al. (14) investigated the effects of severe aortic stenosis (AS) disease on hemodynamic blood flow distribution using CFD approach. The results proved that the norm of blood distribution at carotid branches is affected due to the severity of AS and leads to unequal distribution of blood supply to the important organs of the human body (15). Basri et al. (16) further the investigation on the effect of paravalvular leakage (PVL) issue of Transcatheter Aortic Valve Implantation (TAVI) where the results showed that the existence of PVL in TAVI has developed recirculation flow proximal to the ascending aorta region due to the confluence of high velocity at the center of valve opening and low velocity at the PVL region. In another study, Zakaria et al. (17–20) conducted a Cartesian non-boundary fitted grid method of blood flow in the aorta using OpenFOAM and developed new non body fitted – volume of fluid (NBF-VOF) to solve the problem of the flow on the stationary body on a fixed grid.

The study of stenosed RA condition particularly on hemodynamics blood behavior due to the stenosed of vessel using CFD and FSI approaches had been done by several researchers (6,21–23). For example, Khader et al. (21) compared the hemodynamic behavior of RA with the cases of normal, single stenosed (SS) and double stenosed (DS) for resting and exercise conditions using CFD approach. Authors concluded that, maximum wall shear stress (WSS) occurred at both single and double stenosed compared to normal cases. Moreover, exercise conditions produced high velocity blood flow compared to the rest condition. Basri et. al (24) further this study using FSI approach with normal blood pressure (NBP) and high blood pressure (HBP) condition for normal and SS cases. The results showed that SS-HBP performed the highest maximum magnitude of velocity, von misses stress, pressure, WSS arterial and wall deformation compared to the others. The latest study by Basri et. al (25) conducted CFD study of SS and DS cases of RA stenosed with NBP and HBP condition. The results concluded that the DS-HBP produced the highest maximum pressure and WSS magnitude compared to the others.

In the present work, further investigation of SS-NBP, SS-HBP, DS-NBP and DS-HBP of stenosed RA will be conducted using FSI approach. The simulation provides

advantages for the medical expertise to understand not only focusing on blood flow’s behaviour, hence the structural behaviour of RA tissue due to the impact of fluid flow will be studied in this research.

MATERIALS AND METHODS

Patient Specific Aorta Model

The details construction of the 3D geometry of idealistic abdominal with the renal branch with SS and DS cases is explained in (21,24,26).

Mesh Study

The grid dependency was conducted by comparing the mesh elements with the results of maximum velocity (25) and maximum WSS magnitude (refer Figure 1e). The best selection of mesh for the fluid domain was approximated around 385000 and 394500 for the structural domain of both single and double stenosed models, respectively.

Boundary Condition

The CFD solved the governing Navier Stokes equation of fluid motion in this study are as follows:

$$\nabla \cdot \vec{v} = 0 \quad \text{Continuity (1)}$$

$$\frac{\alpha^2}{Re} \iiint_v \frac{\partial \vec{v}}{\partial t} + \iiint_v (\vec{v} \cdot \nabla) \vec{v} = - \iint_s p \cdot dA + \frac{1}{Re} \iint_s \tau \cdot dA \quad \text{Momentum (2)}$$

Where, τ is the viscous stress tensor; p is the pressure; $Re = \frac{U \cdot R}{\nu}$ is the Reynolds number; $\alpha = \frac{\omega}{v}$ is the Womersley parameter; U is the maximum inlet velocity; R is the aorta inlet radius; ν is the kinematic viscosity; ω is the inlet pulse frequency ($\omega = 2\pi f$; f is the heart rate).

Fluid Domain

For the boundary condition of fluid domain, the velocity inlet and pressure outlet were specified with the condition of pulsatile blood flow as referring to Basri et al. (25) (Figure 1(a & b)). The inlet flow was selected to be incompressible and Newtonian due to the higher relative shear rate ratio above 100 s^{-1} (27). The blood density and dynamic viscosity were selected to be 1050 kg/m^3 and $0.004 \text{ Pa}\cdot\text{s}$, respectively (14,16,25). The arterial wall of fluid domain was set as dynamic mesh with layering and re-meshing technique. The solver of Coupled Scheme with Second Order Upwind of pressure, momentum and turbulent kinetic energy were setup for obtaining accurate results. The k- ω Shear Stress Transport (SST) turbulent model was selected by referring to Basri et al. (15,24,25). The pulsatile time varying velocity profile was applied at the inlet (refer Figure 1c), while two different pulsatile pressure of NBP and HBP conditions were selected as the outlet condition in this simulation (Figure 1d). The three complete cardiac cycles for a total simulation time of 3s with 0.05s time step was carried out during this study. The number of step of each time step was fixed at 30 number of step in order to ensure each time step reached the RMS residual convergence.

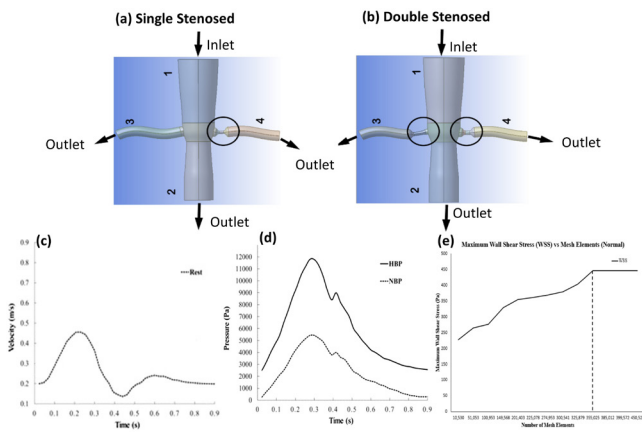


Figure 1: Geometric description of (a) SS and (b) DS (c) Pulsatile velocity applied at inlet (d) Pulsatile pressure applied at outlet (e) Mesh dependency of maximum WSS

The solution converged at 10^{-6} with a duration of 168 hours. The early systole (ES), peak systole (PS), early diastole (ED) and late diastole (LD) were selected as the time points of pulsatile flow for the result observation.

Structural Domain

For structural domain, the arterial wall is assumed to behave linearly-elastic with density of 1120 kg/m^3 , Poisson’s ratio of 0.40 and elastic modulus is 0.9 MPa (28). In this study, the structural wall deformed with response towards the fluid pressure from fluid domain. The number of time step and sub step were set to be similar as the setup of fluid domain.

Fluid Structure Interaction Interface

In this study, the two-way coupling approach was selected which interrelated between the fluid pressure acting at arterial wall and structural deformation of arterial wall, which mimicking the real situation of RA. The time step was set to be 0.05s with total duration of

3s. The response for fluid domain is set at the arterial wall surface, while for structural domain is set at the inner surface of arterial wall. The fluid pressure and structural deformation of both arterial wall surface are changed consecutively subjected to each time step and thus, provide a result of two-way coupling approach.

RESULTS

Numerical simulation of SS and DS models with NBP and HBP of RA were carried out for three pulse cycle. The last cycle was considered and results obtained were taken for further investigation. The hemodynamics parameters such as velocity, pressure, and WSS are studied at specific instants of pulse cycle like ES, PS, ED and LD. These parameters vary with time due to the pulsatility of the flow waveform and the maximum value generally occurred at the peak systole when the inflow is maximum.

Velocity Magnitude

Figure 2(a) shows the comparison of velocity contour of blood flow in the abdominal aorta and renal branches of SS-NBP, SS-HBP, DS-NBP and DS-HBP at PS state. It described the flow separation such that the flow divides into two streams with maximum velocity at the distal wall of the renal bifurcation and slower moving fluid on the proximal wall (24–26). The qualitative results showed a significant difference in velocity contour at the left and right renal arteries between the SS and DS cases. The DS produced lower velocity contour at the left and right renal artery compared to SS due to the effect of stenosed at the renal artery vein which obstructs the blood flow passing through the acute diameter of stenosed. Hence, the balance of the blood flow supplied at the downward of the abdominal aorta. Indeed, the highest magnitude of velocity contour occurs at PS state compared to the other states. Meanwhile, Figure

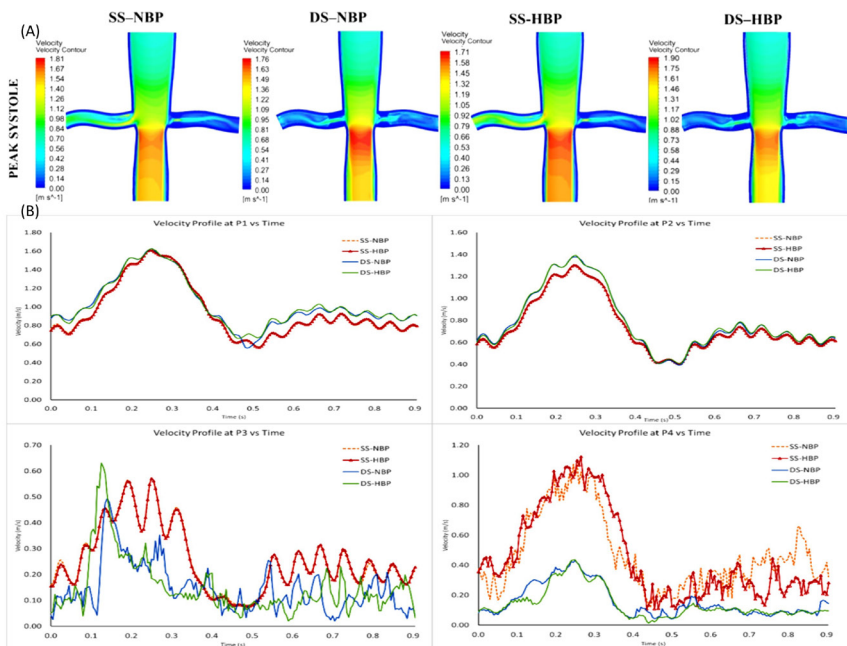


Figure 2: (a) Velocity contour throughout renal artery of SS and DS for NBP and HBP condition at PS state. (b) Maximum velocity of SS and DS for NBP and HBP at P1-P4 location.

2(b) represents the quantitative data of the velocity profile of 4 locations which are P1-P4 (refer Figure 1). At P1 location, the velocity profile for 4 cases showed slightly different at the systolic phase but a bit higher at the diastolic phase especially for DS-NBP and DS-HBP. Meanwhile at P2 location, the results showed vice versa where the DS-NBP and DS-HBP showed a slightly higher velocity profile at the systolic phase rather than the diastolic phase. At P3 location, the velocity profile for SS-NBP and SS-HBP showed higher value compared to DS-NBP and DS-HBP for both systolic and diastolic phases. On the other hand, at P4 location which is at the right RA stenosed, the velocity profile of SS-NBP and SS-HBP showed almost 3 times higher than the velocity profile of DS-NBP and DS-HBP for both systolic and diastolic phase.

Pressure Drop

Figure 3 shows the pressure contour of SS-NBP, SS-HBP, DS-NBP and DS-HBP at PS state. It can be observed that at SS case, the pressure contour acting at the entrance of left and right RA for HBP produced a higher magnitude of pressure contour compared to the NBP condition. Meanwhile, in terms of pressure drop value, for SS case, the pressure drop of right stenosed RA produced higher value compared to the left RA location. At the right RA location, SS-HBP shows the highest pressure drop value with 419.50 MPa compared with SS-NBP with 341.37 MPa. Meanwhile, at the left RA location, the pressure drop value shows a small difference between SS-HBP and SS-NBP with 229.40 MPa and 224.44 MPa, respectively. On the other hand, for the DS case, the pressure drop between the left RA and right RA for DS-NBP and DS-HBP showed small changes. At the left RA location, the pressure drop for DS-HBP shows a lower value with 185.80 MPa compared to DS-NBP with 199.80 MPa. On the other hand, at the right RA location, the pressure drop of DS-HBP shows slightly higher than DS-NBP with 243.20 MPa and 237.40 MPa, respectively.

Time Average Wall Shear Stress (TAWSS) and Oscillatory shear index (OSI)

TAWSS represents the spatial variation of WSS (29,30), as in Figure 4 (a). The contour plot of the TAWSS distribution along aorta is represented SS-NBP, SS-HBP, DS-NBP and DS-HBP. The limit of the legend is set to the maximum magnitude of 7 Pa by referring to W.N. W. A. Naim et. al (30), where the TAWSS magnitude for normal arterial wall is in the range of 1-7 Pa. Hence, by referring to Figure 4 (a), the red contour acting at the abdominal aorta and RA indicate the higher value of TAWSS compared to the normal arterial wall range. It is observed that for each case, higher TAWSS contour acting in the middle of the abdominal aorta and also the stenosed right and left RA. The overall distribution of TAWSS contour for HBP condition showed a higher magnitude than the NBP condition. Quantitatively, the highest TAWSS is found acting at the right RA particularly for SS-HBP with 14.47 Pa followed by SS-NBP, DS-NBP and DS-HBP with 13.26 Pa, 10.57 Pa and 10.07 Pa, respectively. It can be observed that SS has a higher TAWSS value than DS. This is due high concentration of pressure acting at the narrow blood vessel of SS compared to DS cases which most of the blood will flow to the lower part of the abdominal aorta.

Figure 4 (b) shows the OSI contour of SS-NBP, SS-HBP, DS-NBP and DS-HBP. OSI is a measure of the oscillatory nature of shear forces (31). The range between 0 and 0.5 indicates the fraction of the cardiac cycle over instantaneous shear force vector forms. According to Fuch et. al (29), high OSI (over 0.5) has a higher risk for the progression of atherosclerosis. Referring to Figure 4 (b), it is observed that SS-NBP and SS-HBP produced higher OSI value compared to DS-NBP and also DS-HBP. The location of high OSI can be seen acting at the right RA and also the lower part of the abdominal aorta.

Total Deformation

Figure 5 (a) shows the total deformation contour of SS-

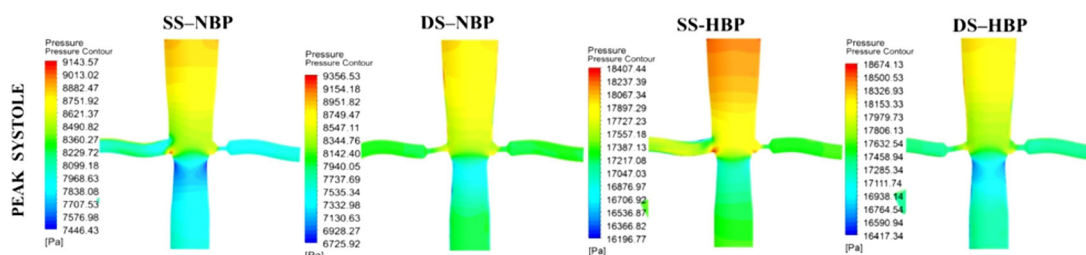


Figure 3: Pressure contour throughout renal artery of SS and DS of NBP and HBP conditions at PS state

Table I: Pressure Drop

Condition / Parameter	SS-NBP		SS-HBP		DS-NBP		DS-HBP	
Pressure Drop (Pa)	Left RA	Right RA						
	224.44	341.37	229.40	419.50	199.80	237.74	185.80	243.20

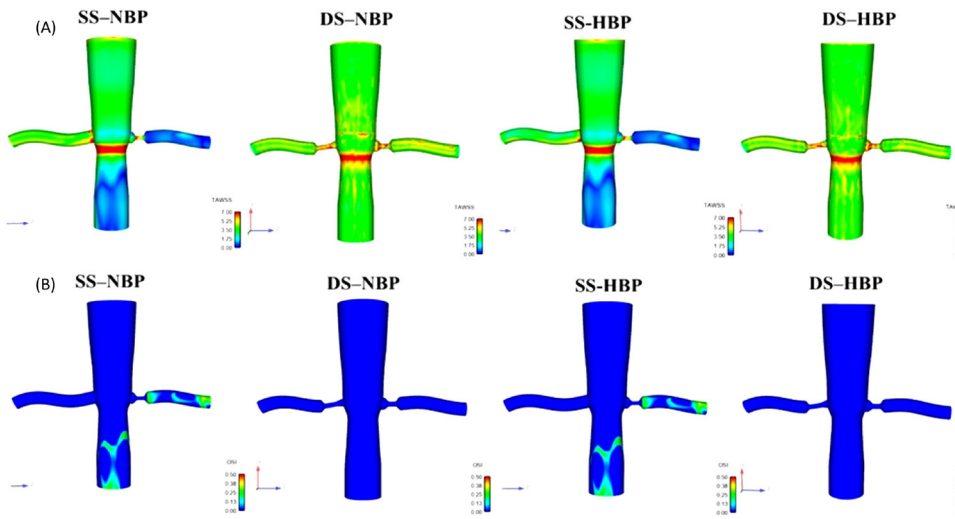


Figure 4: (a) TAWSS contour throughout renal artery of SS and DS (b) OSI contour throughout renal artery of SS and DS

NBP, DS-NBP, SS-HBP and DS-HBP at PS state. From the observation, it can be noticed that the maximum deformation acting at the upper part of the abdominal aorta with the SS-HBP and DS-HBP show the highest maximum deformation distribution compared with SS-NBP and DS-NBP. Moreover, it is observed that the SS-HBP and DS-HBP have a higher distribution of deformation contour compared to SS-NBP and DS-NBP. Quantitatively, at PS state, DS-HBP produced the highest value of maximum deformation with 0.251 mm followed by SS-HBP with 0.224 mm. For the NBP condition, the maximum deformation for DS-NBP and SS-NBP stated to be 0.126 mm and 0.110 mm, respectively which are lower than the HBP condition with almost half fold (refer Figure 5 (b)).

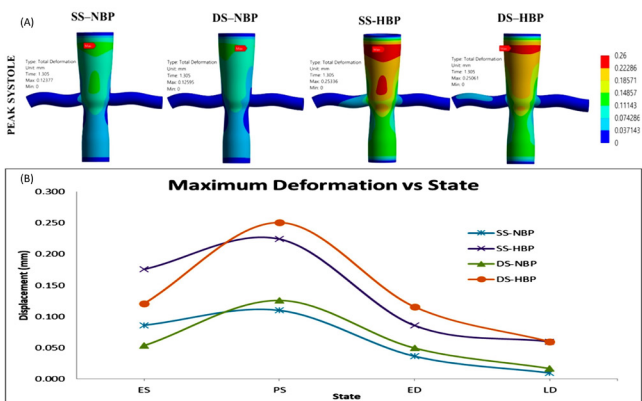


Figure 5: (a) Total Deformation contour throughout renal artery of SS and DS at PS state (b) Maximum Total Displacement of SS and DS for NBP and HBP condition

Von Misses Stress (VMS)

Figure 6 (a) shows the VMS contour of SS-NBP, DS-NBP, SS-HBP and DS-HBP at PS state. From the observation, it can be noticed that the maximum VMS acting at the upper part of the abdominal aorta with the SS-HBP and DS-HBP showed the highest maximum VMS distributions compared with SS-NBP and DS-NBP. Moreover, the VMS distribution on the left and right RA of DS-HBP

showed huge contour changes from high value to lower value of VMS contour due to the existence of stenosis. Quantitatively, at PS state, SS-HBP produced the highest value of maximum VMS with 0.646 MPa followed by DS-HBP with 0.442 MPa. For the NBP condition, the maximum VMS magnitude for SS-NBP and DS-NBP stated to be 0.296 MPa and 0.211 MPa, respectively. It can be observed that the VMS magnitude for HBP condition are two-fold compared to NBP condition (refer Figure 6 (b)).

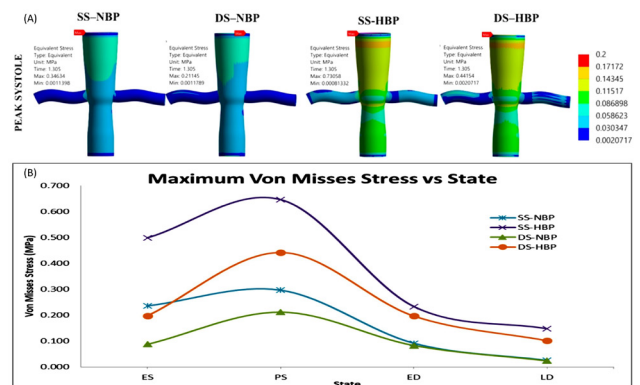


Figure 6: (a) VMS contour of SS and DS for NBP and HBP condition at PS state (b) Maximum VMS of SS and DS for NBP and HBP condition

DISCUSSION

The velocity profile of DS-NBP and DS-HBP showed almost 3 times lower than the velocity profile of SS-NBP and SS-HBP for both systolic and diastolic phase. This has proven that the existence of stenosed at both RA locations have a higher impact on the velocity magnitude reduction. The reduction of velocity magnitude has decreased the blood flow movement towards the RA branches which affected the blood supply towards kidney, hence it will lead towards chronic kidney failure (2). On the other hand, the existence of stenosis produced higher pressure drop value compared to the

normal vessel condition. SS-HBP showed the highest pressure drop value with 419.50 MPa compared to the others. This circumstances may cause the RA wall to be collapsed due to high pressure loss which augmented the flow resistance (30). The location of high TAWSS and OSI can be seen acting at the right RA and also the lower part of the abdominal aorta. This indicates that high OSI increased residence time to interact with the arterial vessel wall. Hence, it leads to the development of plaque formation, stimulates platelet aggression and thrombus formation Liu et. al (32). For total deformation, the HBP condition has a higher impact of renal artery wall displacement compared to NBP where DS produced slightly higher deformation value compared to SS case. Moreover, the HBP condition has a higher impact of RA VMS magnitude compared to NBP where SS-HBP produced higher VMS value compared to the DS-HBP case.

CONCLUSION

In this study, an investigation between SS and DS of NBP and HBP conditions in terms of blood flow behaviour and RA wall tissue structural behaviour had been conducted using the aid of the FSI simulation approach. From this study, for blood flow behaviour, it can be concluded that SS-NBP and SS-HBP produced a higher value of velocity profile parameter compared to DS-NBP and DS-HBP at left and right stenosed RA. Moreover, SS-HBP indicates the highest value of pressure drop followed by DS-HBP particularly at the right stenosed RA location. For TAWSS and OSI parameter, SS-NBP showed the highest value compared to the others. Meanwhile, for the RA wall tissue behaviour, the SS-HBP and DS-HBP have a higher distribution of deformation contour and also maximum VMS compared to SS-NBP and DS-HBP. This has proven that the existence of SS at RA location has a higher impact on the velocity magnitude, higher pressure drop, higher TAWSS and OSI value compared to the DS case. This is due to a high concentration of pressure acting at the narrow blood vessel of SS compared to DS cases which most of the blood flow will pass to the lower part of abdominal aorta. Besides, the HBP condition provide a higher impact of renal artery wall displacement and VMS compared to NBP condition.

ACKNOWLEDGEMENT

This work is supported by UPM under GP-IPM grant, 9675000. The authors would like to express their gratitude and sincere appreciation to Department of Aerospace Engineering, Faculty of Engineering, Universiti Putra Malaysia for the close collaboration in this work.

REFERENCES

1. Albert S, Balaban RS, Neufeld EB, Rossmann JS. Influence of the renal artery ostium flow diverter

on hemodynamics and atherogenesis. *J Biomech* [Internet]. 2014;47(7):1594–602.

2. Bokhari MR, Bokhari SRA. Renal Artery Stenosis. *StatPearls* [Internet] StatPearls Publ. 2019;571–9.
3. Wang M, Sun S, Ren Y. The value of contrast-enhanced ultrasound in the evaluation of accessory renal artery in patients with suspected renal artery stenosis. *Zhonghua Yi Xue Za Zhi*. 2019;99(11):838–40.
4. Moore JE, Xu C, Glagov S, Zarins CK, Ku DN. Fluid wall shear stress measurements in a model of the human abdominal aorta: oscillatory behavior and relationship to atherosclerosis. *Atherosclerosis*. 1994;110(2):225–40.
5. Zhang W, Qian Y, Lin J, Lv P, Karunanithi K, Zeng M. Hemodynamic analysis of renal artery stenosis using computational fluid dynamics technology based on unenhanced steady-state free precession magnetic resonance angiography: Preliminary results. *Int J Cardiovasc Imaging*. 2014;30(2):367–75.
6. Mortazavinia Z, Zare A, Mehdizadeh A. Effects of renal artery stenosis on realistic model of abdominal aorta and renal arteries incorporating fluid-structure interaction and pulsatile non-Newtonian blood flow. *Appl Math Mech (English Ed)*. 2012;33(2):165–76.
7. Kagadis GC, Skouras ED, Bourantas GC, Paraskeva CA, Katsanos K, Karnabatidis D, et al. Computational representation and hemodynamic characterization of in vivo acquired severe stenotic renal artery geometries using turbulence modeling. *Med Eng Phys*. 2008;30(5):647–60.
8. Suh GY, Les AS, Tenforde AS, Shadden SC, Spilker RL, Yeung JJ, et al. Hemodynamic changes quantified in abdominal aortic aneurysms with increasing exercise intensity using MR exercise imaging and image-based computational fluid dynamics. *Ann Biomed Eng*. 2011;39(8):2186–202.
9. Suh GY, Les AS, Tenforde AS, Shadden SC, Spilker RL, Yeung JJ, et al. Quantification of particle residence time in abdominal aortic aneurysms using magnetic resonance imaging and computational fluid dynamics. *Ann Biomed Eng*. 2011;39(2):864–83.
10. Marshall I, Zhao S, Papatheanasopoulou P, Hoskins P, Xu XY. MRI and CFD studies of pulsatile flow in healthy and stenosed carotid bifurcation models. *J Biomech*. 2004;37(5):679–87.
11. Wong KKL, Dong J, Tu J. Numerical study of stenosed carotid bifurcation models based on wall shear stress distribution. *2nd Int Conf Biomed Eng Technol*. 2012;34:1362–70.
12. Taylor CA, Draney MT. Experimental and Computational Methods in Cardiovascular Fluid Mechanics. *Annu Rev Fluid Mech*. 2004;36(1):197–231.
13. Hussain SA, Tat TH, Hamid MIA, Abdullah N,

- Idris A. Pressure reduction on blood flow in aorta coronary sinus conduit. *Pertanika J Sci Technol*. 2012;20(2):347–53.
14. Basri AA, Zuber M, Zakaria MS, Illyani E, Fazli A, Aziz A, et al. The Effects of Aortic Stenosis on the Hemodynamic Flow Properties using Computational Fluid Dynamics. *Int J FLUIDS HEAT Transf*. 2016;1(3):33–42.
 15. Basri AA, Zubair M, Aziz AFA, Ali RM, Tamagawa M, Ahmad KA. Computational Fluid Dynamics Study of the Aortic Valve Opening on Hemodynamics Characteristics. In: *IEEE Conference on Biomedical Engineering and Sciences*, 8 - 10 December 2014, Miri, Sarawak, Malaysia. 2014. p. 99–102.
 16. Basri AA, Zuber M, Zakaria MS, Basri EI, Fazli A, Aziz A, et al. The Hemodynamic Effects of Paravalvular Leakage Using Fluid Structure Interaction: Transcatheter Aortic Valve Implantation Patient. *J Med Imaging Heal Informatics*. 2016;6(6):1513–8.
 17. Zakaria MS, Ismail F, Tamagawa M, Aziz AFA, Wiriadidjaja S, Basri AA, et al. A Cartesian non-boundary fitted grid method on complex geometries and its application to the blood flow in the aorta using OpenFOAM. *Math Comput Simul [Internet]*. 2019;159:220–50.
 18. Zakaria MS, Ismail F, Tamagawa M, Aziz AFA, Wiriadidjaja S, Basri AA, et al. Review of numerical methods for simulation of mechanical heart valves and the potential for blood clotting. Vol. 55, *Medical and Biological Engineering and Computing*. Springer Berlin Heidelberg; 2017. 1519–1548 p.
 19. Zakaria MS, Ismail F, Tamagawa M, Fazli A, Azi A, Wiriadidjaya S, et al. Computational Fluid Dynamics Study of Blood Flow in Aorta using OpenFOAM. *J Adv Res Fluid Mech Therm Sci J homepage [Internet]*. 2018;43(May):81–9.
 20. Zakaria MS, Ismail F, Tamagawa M, Aziz AFA, Wiriadidjaya S, Basri AA, et al. Numerical Analysis Using a Fixed Grid Method for Cardiovascular Flow Application. *J Med Imaging Heal Informatics*. 2016;6(6):1483–8.
 21. Khader SMA, Azriff A, Pai R, Zubair M, Ahmad KA, Ahmad Z, et al. Haemodynamics study in subject-specific abdominal aorta with renal bifurcation using CFD - A case study. *J Adv Res Fluid Mech Therm Sci*. 2018;50(2):118–21.
 22. Taylor CA, Hughes TJR, Zarins CK. Finite element modeling of three-dimensional pulsatile flow in the abdominal aorta: Relevance to atherosclerosis. *Ann Biomed Eng*. 1998;26(6):975–87.
 23. LIANG F, YAMAGUCHI R, LIU H. Fluid Dynamics in Normal and Stenosed Human Renal Arteries: an Experimental and Computational Study. *J Biomech Sci Eng*. 2006;1(1):171–82.
 24. Basri AA, Mohammed S, Khader A, Johny C, Pai R, Zuber M, et al. Numerical Study of Haemodynamics Behaviour in Normal and Single Stenosed Renal Artery using Fluid-Structure Interaction. *J Adv Res Fluid Mech Therm Sci J homepage [Internet]*. 2018;51(1):91–8.
 25. Basri AA, Khader SMA, Johny C, B RP, Zuber M, Ahmad Z, et al. Effect of Single and Double Stenosed on Renal Arteries of Abdominal Aorta : A Computational Fluid Dynamics. 2020;1(1):87–97.
 26. Khader SMA, Azriff A, Johny C, Pai R, Zuber M, Ahmad KA, et al. Haemodynamics behaviour in normal and stenosed renal artery using computational fluid dynamics. *J Adv Res Fluid Mech Therm Sci*. 2018;51(1):80–90.
 27. Basri AA, Zuber M, Basri EI, Zakaria MS, Aziz AFA, Tamagawa M, et al. Fluid Structure Interaction on Paravalvular Leakage of Transcatheter Aortic Valve Implantation Related to Aortic Stenosis: A Patient-Specific Case. *Comput Math Methods Med [Internet]*. 2020.
 28. Azriff A, Johny C, Khader SMA, B RP, Zuber M, Ahmed KA. Numerical Study of Haemodynamics in Abdominal Aorta with Renal Branches Using Fluid – Structure Interaction under Rest and Exercise Conditions. 2018;(4):23–7.
 29. Fuchs A, Berg N, Wittberg LP. Stenosis indicators applied to patient-specific renal arteries without and with stenosis. *Fluids*. 2019;4(1).
 30. Wan Ab Naim WN, Ganesan PB, Sun Z, Osman K, Lim E. The impact of the number of tears in patient-specific Stanford type b aortic dissecting aneurysm: CFD simulation. *J Mech Med Biol*. 2014;14(2).
 31. Singh PK, Marzo A, Howard B, Rufenacht DA, Bijlenga P, Frangi AF, et al. Effects of smoking and hypertension on wall shear stress and oscillatory shear index at the site of intracranial aneurysm formation. *Clin Neurol Neurosurg [Internet]*. 2010;112(4):306–13.
 32. Liu M, Sun A, Deng X. Hemodynamic effect of obstruction to renal arteries caused by stent grafts in patients with abdominal aortic aneurysms. *J Mech Med Biol*. 2018;18(7):1–14.